Scientific Reports

https://doi.org/10.1038/s41598-026-57286-8

Article in Press

Thermal management of pouch-type lithium-ion batteries using aluminum oxide porous media filled with nano-enhanced PCM

Received: 10 November 2025

Accepted: 5 June 2026

Published online: 01 July 2026

Cite this article as: Alromithy F.S., Ali A.B.M., Alkhatib O.J. *et al.* Thermal management of pouch-type lithium-ion batteries using aluminum oxide porous media filled with nano-enhanced PCM. *Sci Rep* (2026). https://doi.org/10.1038/s41598-026-57286-8

Fares Suliaman Alromithy, Ali B. M. Ali, Omar J. Alkhatib, Pradeep Kumar Singh, Shimaa A. Hussien, Hamdi Ayed, Farzona Tursunzoda, Mahidzal Dahari & Ibrahim Mahariq

Thermal Management of Pouch-Type Lithium-Ion Batteries Using Aluminum Oxide Porous Media Filled with Nano-Enhanced PCM

Fares Suliaman Alromithy [1], Ali B. M. Ali [2], Omar J. Alkhatib [3], Pradeep Kumar Singh [4], Shimaa A. Hussien [5], Hamdi Ayed [6], Farzona Tursunzoda [7], Mahidzal Dahari [8], Ibrahim Mahariq [9, 10]

[1] Assistant Professor, Department of Electrical Engineering, University of Tabuk, Tabuk, Saudi Arabia

[2] Advanced Technical College, University of Warith Al-Anbiyaa, Karbala, Iraq

[3] Architectural Engineering Department, College of Engineering, UAE University, United Arab Emirates

[4] Department of Mechanical Engineering, Institute of Engineering & Technology, GLA University, Mathura (U.P.)-281406, India

[5] Electrical Department, Faculty of Engineering, Princess Nourah Bint Abdulrahman University, P.O. Box 84428, 11671, Riyadh, Saudi Arabia

[6] Department of Civil Engineering, College of Engineering, King Khalid University, Abha – 61421, Saudi Arabia

[7] College of Science and Technology, University of Rwanda, Kigali, Rwanda

[8] Department of Electrical Engineering, Faculty of Engineering, Universiti Malaya, 50603, Kuala Lumpur, Malaysia

[9] University College, Korea University, Seoul 02481, South Korea

[10] Department of Medical Research, China Medical University Hospital, China Medical University, Taichung, Taiwan

Main corresponding author: Mahidzal Dahari (mahidzal@um.edu.my)

Co-corresponding author: Ibrahim Mahariq (mahariq@korea.ac.kr)

Abstract

This study presents a novel battery thermal management approach for large-format pouch-type lithium-ion batteries (LIBs) commonly used in electric vehicles. A composite housing structure consisting of Al_2O_3 foam filled with a nano-enhanced phase change material (NPCM), a mixture of n-octadecane and copper nanoparticles, was investigated using numerical simulations under different C-rates (0.5C, 1C, 1.5C, and 2C) and foam porosities (0.90, 0.92, 0.94, 0.96, and 0.98). The Al_2O_3 foam increases the effective surface area and thermal conductivity, while the copper nanoparticles mitigate the low thermal conductivity of pure PCM. Results show that this hybrid system significantly reduces maximum battery temperature, delays temperature rise through latent heat absorption, and improves temperature uniformity. Increasing the C-rate, especially from 1.5 to 2, intensifies heat generation, while lower porosity ($\varepsilon = 0.9$) enhances thermal performance by redistributing heat toward the cell center. The proposed NPCM–Al_2O_3 foam configuration

offers a promising strategy to enhance the safety, efficiency, and longevity of high-capacity LIBs in electric vehicle applications.

Keywords: *BTMS, pouch lithium-ion battery, NPCM,* Al_2O_3*, copper particles.*

1 Introduction

The adoption of electric vehicles (EVs) is a key strategy to reduce greenhouse gas emissions and urban air pollution [1-4]. EVs can also reduce dependence on fossil fuels and enable cleaner transportation when coupled with renewable electricity [5-7]. Lithium-ion batteries, including cylindrical and pouch-type formats, are central to EV operation; however, their performance, lifetime, and safety are highly temperature dependent, making Battery Thermal Management Systems (BTMS) essential to prevent overheating and thermal runaway [8-11].

The main objective of BTMS research is to maintain a stable operating temperature during charge and discharge. Accordingly, several approaches have been proposed, including air-based cooling systems [12], conductive enhancements such as fins [13], porous media coverings [14], and phase change materials (PCMs) [15-19]. PCM-based BTMS has received considerable attention because latent heat storage enables passive thermal regulation with silent operation and no additional power consumption [20]. Nevertheless, the low thermal conductivity of most conventional PCMs limits heat spreading and can reduce cooling effectiveness under high heat generation [21]. To address this limitation, hybrid designs have been explored by combining PCMs with forced convection [13, 22, 23] or conductive structures such as metal fins or foams to enhance heat transfer and improve temperature uniformity.

These studies have evaluated various fin geometries, including straight [24], circular [25, 26], arc-shaped [27], helical [28], triangular [29, 30], I-shaped [30], and complex Y-, N-, and Z-shaped designs [31]. In addition to reassessing these simpler configurations, Liu et al. [32] conducted further analysis on more intricate aluminum fin structures to assess their influence on the heat dissipation capabilities of PCMs. Their findings highlighted that bifurcated fin configurations, notably the two-branch variation, were most effective in lowering battery temperatures. Moreover, although adding more fins tends to enhance cooling, adjusting the PCM layer thickness did not

show a significant impact on overall thermal efficiency. Xiang et al. [33] investigated a hybrid BTMS that combines forced cooling with a composite PCM. They reported that the system maintains the pack temperature within an acceptable range at constant C-rates below ~15C, whereas at >15C the PCM is depleted quickly and higher coolant flow is required. Under dynamic cycles, they also showed improved control when the charge rate is kept low, and concluded that higher-latent-heat CPCMs can further delay PCM depletion and extend high-rate capability. On the other hand, based on previous research, the presence of pores in a metal matrix increases the effective surface area between the solid structure and the working fluid, thereby promoting convective heat transfer. The interconnected pore network facilitates uniform fluid flow, minimizing stagnant zones and improving overall heat transfer performance. Moreover, the use of copper foam can generate localized turbulence, disrupt the boundary layer, and further enhance thermal exchange efficiency [34-37]. Salami Ranjbaran et al. [38] investigated the effect of incorporating copper foam at varying volume fractions (1–9 vol%) into paraffin wax, a commonly used PCM, to enhance its thermal conductivity. Through numerical simulations of nine passive BTMS configurations, they found that the addition of 6 vol% copper foam yielded the most effective cooling performance, successfully maintaining the battery temperature within a safe operating range. However, increasing the copper foam content beyond this level diminished the PCM's latent heat storage capacity, thereby reducing the overall reliability of the system. Sudhakaran et al. [39] investigated how various factors, including PCM type, thickness, copper foam content, and heat transfer coefficient, affect the cooling performance of PCMs in BTMS, using numerical simulations conducted in ANSYS Fluent. The PCMs examined were Capric Acid, RT-35, RT-42, and RT-55, with thicknesses ranging from 2 mm to 8 mm and heat transfer coefficients between 5 and 11 $W/m^2 \cdot K$. Copper foam was added as a conductive enhancer at volume fractions of 1%, 3%, 5%, and 7%. Among the tested configurations, the fourth combination, using Capric Acid, achieved the lowest cell temperature (303.088 K), while RT-35 also demonstrated strong thermal performance. ANOVA analysis revealed that PCM material had the greatest impact on cooling efficiency (35.4%), followed closely by PCM thickness (35.13%), with heat transfer coefficient (13.98%) and additive content (5.09%) having comparatively lesser effects.

In recent years, researchers have explored the incorporation of nanoparticle-enhanced phase change materials (NPCMs) to further enhance the thermal performance of battery systems [40-43].

The addition of nanoparticles (NPs) with high thermal conductivity to the PCM matrix significantly increases the overall thermal conductivity of the material. This enhancement enables faster heat dissipation and more efficient thermal regulation within the battery system. Additionally, the presence of NPs can act as nucleation sites, promoting uniform phase transitions and reducing the risk of hotspot formation [44-47]. As previously discussed, incorporating thermal conductivity enhancers into composite PCMs is an effective strategy for improving their heat transfer capabilities. These enhancers are generally categorized as either metallic or non-metallic, with copper being the most commonly used metallic additive. Pan et al. [48] developed a BTMS utilizing a cut copper fiber sintered skeleton (CCFSS)/paraffin composite PCM, which significantly enhanced thermal conductivity and maintained the cell temperature variation within 5□°C. Similarly, Karimi et al. [49] introduced a metal matrix along with metal nanoparticles into the PCM, achieving a 70% reduction in the maximum temperature difference between the battery and the PCM surface. Furthermore, composites incorporating silver nanoparticles demonstrated superior thermal performance. Mehrabi et al. [41] incorporated paraffin into a copper foam matrix, which effectively maintained the temperature below 60□°C even under high discharge conditions. However, the system demonstrated reduced efficiency when operating at an ambient temperature of 40□°C. Among metal-based additives, aluminum and aluminum-containing materials remain the most commonly employed. Zou et al. [50] reported that a composite phase change material containing multi-walled carbon nanotubes (MWCNTs) and graphene in a mass ratio of 3:7 exhibited the most effective heat transfer performance. This formulation significantly enhanced thermal conductivity compared to PCMs incorporating only graphene or only MWCNTs, with improvements of 31.8% and 55.4%, respectively, while also mitigating the rapid temperature rise associated with liquid PCMs. Additionally, silicone has been identified as another effective additive for enhancing thermal conductivity. Righetti et al. [51] investigated the use of metal meshes with varying pore sizes to enhance the thermal conductivity of PCMs. Their findings demonstrated that aluminum-based mesh structures significantly improved both the charging and cooling processes. In another study, Li et al. [52] embedded battery cells within a PCM composite containing Al_2O_3 and arranged them into arrays. Upon exposure to airflow, it was observed that power consumption during charging was lowest at a Reynolds number of 300 and highest at a Reynolds number of 500. Maintaining safe and uniform temperatures in large-format pouch lithium-ion batteries under high C-rate operation remains a critical challenge for electric-vehicle

thermal management, particularly when passive solutions are preferred to reduce complexity, mass, and parasitic power consumption. Although PCMs can buffer temperature rise through latent heat, their inherently low thermal conductivity limits heat spreading and can lead to localized hot spots, while porous metal/ceramic foams can enhance conduction but require careful design to avoid sacrificing latent heat capacity. Despite the growing interest in nano-enhanced PCMs (NPCMs) and porous media separately, the coupled thermal behavior of porous Al□O□ foam filled with an NPCMs for pouch cells, and the associated trade-offs among peak temperature, temperature uniformity, and latent heat utilization, remain insufficiently quantified, especially across different foam porosities and discharge rates. Motivated by this gap, the present study numerically investigates a hybrid passive cooling concept that integrates Al□O□ porous media with an NPCM based on n-octadecane and copper nanoparticles. The novelty of this work lies in systematically quantifying how foam porosity and C-rate jointly influence heat dissipation, melting dynamics (latent heat utilization), and temperature non-uniformity in a large-format pouch cell, thereby providing design-oriented insights for optimizing NPCM–Al_2O_3foam configurations for practical EV battery thermal management. Key thermal performance parameters, including average and maximum battery temperatures, total melting fraction (TMF) curves, and heat dissipation contours, were examined and discussed in detail.

2 Problem description

As demonstrated in previous studies, Al_2O_3 foam can significantly improve thermal conductivity compared to pure PCM. Furthermore, the incorporation of copper nanoparticles addresses the inherently low thermal conductivity of n-octadecane. To evaluate the effectiveness of this approach, using CFD framework and FVM approach, we conducted numerical simulations to analyze its impact under various charge-discharge rates (C-rates: 0.5, 1, 1.5, and 2) and porosity levels (0.90, 0.92, 0.94, 0.96, and 0.98). The NPCM developed in this work is a composite of n-octadecane and nano-sized copper particles. N-octadecane (C□□H□□) is a paraffin-based PCM widely employed for thermal energy storage due to its high latent heat of fusion (~230–245□kJ/kg) and a melting temperature around 28□°C, making it particularly suitable for applications near room temperature. It also exhibits excellent chemical stability, is non-corrosive, and can undergo numerous melting/solidification cycles without significant degradation. However, the material suffers from low thermal conductivity, which limits the rate of heat transfer during charging and

discharging. To overcome this limitation, we incorporated nano-sized copper particles into the PCM. Copper nanoparticles possess extremely high thermal conductivity (reduced from the bulk value of ~400 W/(m·K) due to surface and grain-boundary effects but still significantly higher than most materials). Their melting point decreases from 1085 °C as the particle size decreases, but they retain superior heat transfer properties. When dispersed in PCMs at low concentrations (1–5 wt%), these nanoparticles greatly enhance the effective thermal conductivity, thereby accelerating the melting and solidification processes [53, 54]. Therefore, copper nanoparticles are widely used in thermal energy storage systems due to their effectiveness and relatively low cost compared to noble metals.

On the other hand, Al O porous media was selected instead of commonly used copper or graphite foams for several practical reasons. Although copper foam provides very high intrinsic thermal conductivity, they are electrically conductive, which may increase the risk of short circuits when integrated near battery terminals and current collectors. In contrast, Al O is electrically insulating, chemically stable, and highly resistant to corrosion, making it more suitable for safe and long-term integration in pouch-type battery modules. Moreover, Al O porous ceramics allow controllable porosity and pore morphology, enabling systematic tuning of effective thermal conductivity and latent heat capacity. While its intrinsic conductivity is lower than that of metallic foams, the balance between safety, thermal stability, and structural tunability makes Al O a promising alternative for hybrid PCM-based BTMS applications.

The synergistic combination of nano-enhanced PCM with Al_2O_3 foam offers an efficient strategy for managing the heat generated by high-capacity pouch-type lithium-ion batteries. The geometry and specifications of the pouch-type lithium-ion battery used in this study are shown in Figure 1 and summarized in Table 1, while the properties of the housing materials, including Al_2O_3 foam, n-octadecane, and copper nanoparticles, are presented in Table 2.

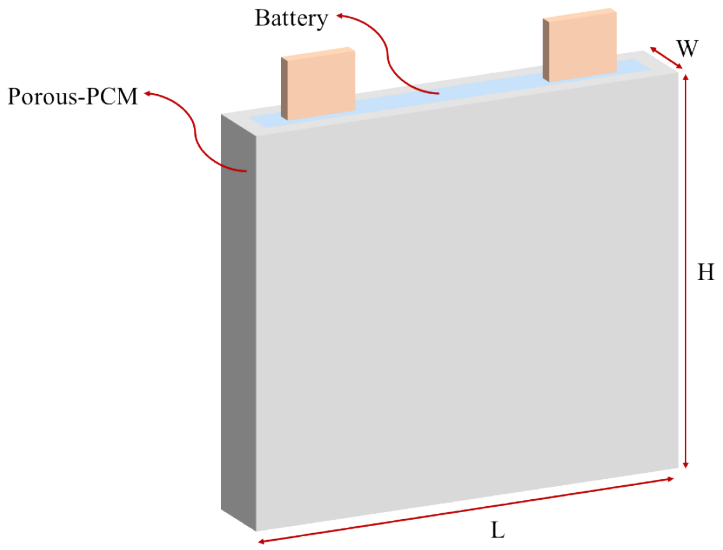

Figure 1: Geometry of high-capacity pouch-type lithium-ion battery.

Table 1:20Ah LIPC specifications [55-58].

Parameter	Value
Specific power (W/kg)	2400
Specific energy (Wh.kg)	131
Size (mm³)	205×157×7
Density (kg/m³)	1940
Thermal conductivity (W/m.K)	18.2
Specific heat capacity (J/kg.K)	1000
Internal resistance (mΩ)	50
Nominal voltage (V)	3.3
Nominal current at 1C (A)	20

Table 2: Speciation of housing materials [58-62].

	$\rho\left(\frac{kg}{m^3}\right)$	$k\left(\frac{W}{m.K}\right)$	$C_p\left(\frac{J}{kg.K}\right)$	$\beta\left(\frac{1}{K}\right)$	$\mu\left(\frac{kg}{ms}\right)$	T_m (K)	T_{mr} (K)	$h\left(\frac{kJ}{kg}\right)$
n_octadecane	747	*0.15*	2127	9.1×10^{-4}	3.86×10^{-3}	301	1.5	243.5

Copper	1356	*398*	*386*	0.17×10^{-4}	-	--	-	-
Aluminum oxide	3970	25	1430	-	-	-	-	-

3 Governing Fluid Dynamics and Heat Transfer Equations

At the beginning of the simulation, a uniform initial temperature of 27 °C is imposed throughout the entire computational domain. The initial velocity is set to zero, as the battery and the Al□O□–PCM composite are treated as a solid/porous structure without any externally imposed flow. Regarding boundary conditions, all external surfaces are considered thermally insulated, meaning no heat flux is allowed to pass through the outer boundaries. For the momentum equations, a no-slip boundary condition is applied wherever velocity terms are present in the numerical formulation. Moreover, for the numerical simulation carried out in this study, a set of simplifying assumptions was applied. The NPCM within the lithium-ion battery was assumed to be incompressible and to exhibit laminar flow behavior, with its thermophysical properties considered constant throughout the process. To capture the dynamics of phase transition, two additional source terms were introduced into the momentum equations: the first term modeled the solidification process occurring as the material changes from liquid to solid, and another to account for buoyancy effects resulting from density variations in the NPCM. Since the system undergoes alternating solid and liquid phases, the influence of latent heat must be incorporated into the energy balance. Accordingly, the energy equation is formulated to include the latent heat associated with the phase change phenomenon [63-66]:

$$\nabla . V = 0 \quad (1)$$

$$\rho_{NPCM}\frac{\partial V}{\partial t} + \rho_{NPCM}(V.\nabla)V = -\nabla p + \mu_{NPCM}\nabla.(\nabla V) + (\rho\beta)_{NPCM}\,(T - T_s)g - 10^5\frac{(1-\lambda)^2}{\lambda^3 + 10^{-3}}V + \frac{\mu_{NPCM}}{K}V \quad (2)$$

$$(\rho C_P)_{eff}\frac{\partial T}{\partial t} + \rho_{NPCM}\left(\varepsilon h_{NPCM}\frac{d\lambda}{dT}\right)\frac{\partial T}{\partial t} + (\rho C_p)_{NPCM}(V.\nabla T) = k_{eff}\nabla.(\nabla T) \quad (3)$$

$$\lambda = 0.5\,erf\left(4\frac{T_s - T_m}{T_l - T_s}\right) + 0.5 \quad (4)$$

In addition, the thermophysical properties of the NPCM must be considered to conduct a comprehensive analysis. Key properties such as density, thermal conductivity, specific heat, thermal expansion coefficient, dynamic viscosity, and enthalpy play a crucial role in formulating the governing equations required to accurately model and predict the behavior of the NPCM within the system [53, 54, 63-67].

$$\rho_{NPCM} = (1 - \varphi)\rho_{PCM} + \varphi\,\rho_{Cu} \quad (5)$$

$$k_{NPCM} = \frac{k_{Cu} + 2k_{PCM} + 2\varphi(k_{Cu} - k_{PCM})}{k_{Cu} + 2k_{PCM} - \varphi(k_{Cu} - k_{PCM})}k_{PCM} \quad (6)$$

$$C_{p,\,NPCM} = \frac{(1 - \varphi)(\rho C_p)_{PCM} + \varphi(\rho C_p)_{Cu}}{\rho_{NPCM}} \quad (7)$$

$$\mu_{NPCM} = \frac{\mu_{PCM}}{(1 - \varphi)^{2.5}} \quad (8)$$

$$\beta_{NPCM} = \frac{(1 - \varphi)(\rho\beta)_{PCM} + \varphi(\rho\beta)_{Cu}}{\rho_{NPCM}} \quad (9)$$

$$h_{NPCM} = (1 - \varphi)h_{PCM} \quad (10)$$

To investigate the thermal behavior of lithium-ion batteries, a set of fundamental parameters is defined. The velocity vector V describes the flow of the cooling medium surrounding the battery,

while t denotes time, which is essential for capturing transient thermal responses. The symbol T corresponds to temperature within the battery, a key factor for both performance optimization and safety evaluation. The variable p stands for pressure, which influences the thermodynamic state of battery materials, and g represents gravitational acceleration, affecting fluid motion around the system. Material properties are also incorporated: ρ denotes density, which determines mass transport and thermal inertia; μ signifies dynamic viscosity, which governs resistance to fluid flow; and β refers to the thermal expansion coefficient, characterizing the volume change of materials with temperature. The specific heat capacity, Cp, represents the amount of heat required to raise the temperature of a unit mass of material, while k indicates thermal conductivity, which controls the efficiency of heat dissipation. The latent heat associated with phase transition is expressed as h, and λ corresponds to the active material fraction, defining the proportion of the battery volume occupied by active materials.

In the effective-property calculations for the NPCM/AOF composite, the Al□O□ foam porous diameter was set to d_p=0.5 mm. Phase change within the PCM domain is modeled using the enthalpy–porosity method, in which latent heat is incorporated through an enthalpy-based energy formulation and the solid–liquid interface is treated as a mushy zone rather than a sharp boundary. In this approach, the solver updates the local liquid fraction (β) at each time step directly from the temperature field using the PCM solidus and liquidus temperatures: β=0 represents fully solid PCM, β=1 represents fully liquid PCM, and intermediate values represent partial melting/solidification within the mushy region. To ensure physically consistent behavior, the momentum equations include a porosity-based damping term that progressively suppresses velocity as the NPCM solidifies, forcing the velocity to approach zero in solid regions while allowing buoyancy-driven flow in the molten PCM. This formulation enables stable tracking of partial or complete melting/solidification under the sub-zero boundary conditions examined in this study and is used to generate the melt-fraction (melting fraction) profiles reported in the results [68-70].

$$(\rho C_P)_{eff} = \varepsilon(\rho C_P)_{PCM} + (1 - \varepsilon)(\rho C_P)_{af} \quad (1)$$

$$k_{eff} = \varepsilon\, k_{PCM} + (1 - \varepsilon)k_{af} \quad (2)$$

$$K = \frac{d_p^2 \varepsilon^3}{150(1 - \varepsilon)^2} \quad (3)$$

Also, the volumetric heat-generation rate of the lithium-ion battery is calculated based on the well-established electrochemical heat-balance formulation**.** The total heat generation consists of two main contributions: a) irreversible heat due to internal resistance and polarization losses and b) reversible (entropic) heat associated with entropy change during lithium intercalation/deintercalation. The irreversible term is proportional to the product of current and overpotential (or internal resistance), while the reversible term depends on the temperature coefficient of the open-circuit voltage. Accordingly, the heat-generation rate in the present study is expressed as the sum of irreversible and reversible components, assuming a uniform current distribution within the cell. This approach has been widely adopted in numerical thermal modeling of lithium-ion batteries and provides a reliable representation of heat production under different discharge C-rates. Therefore, we can use the following equations to calculate heat dissipation generated by the lithium-ion battery [53, 54, 65-67]:

$$(\rho C_{p,c})_c \frac{\partial T_c}{\partial t} = k_c \left(\frac{\partial^2 T_c}{\partial x^2} + \frac{\partial^2 T_c}{\partial y^2} + \frac{\partial^2 T_c}{\partial z^2} \right) + \dot{g}_c \quad (11)$$

$$\dot{g}_c = \frac{1}{V_c} \left(R_c I_c^2 + I_c T_c \frac{dE_{oc}}{dT_c} \right) \quad (12)$$

In this study, $\dot{g}_c$ denotes the heat produced inside the LIC due to two primary sources: its internal electrical resistance and the electrochemical reactions occurring during operation. The portion of heat associated with electrochemical reactions is quantified using the term $\frac{dE_{oc}}{dT_c}$, where dE_{oc} represents the variation in open-circuit voltage and dT corresponds to the change in the LIC's temperature. For these calculations, the entropy coefficient is taken as 0.4 V/K. Furthermore, V_c, R_c, and I_c indicate the volume of the LIC, its internal resistance, and the electric current passing through it, respectively.

4 Simulation process

In this study, computational fluid dynamics (CFD) combined with the finite volume method (FVM) was applied to analyze a prismatic lithium-ion that incorporates an inclined enclosure filled with a NPCM composed of n-octadecane and solid copper nanoparticles. The numerical model was developed to solve the governing equations and investigate the resulting temperature fields and flow patterns. The simulations were carried out using defined boundary conditions and thermophysical parameters, where the effective properties of the NPCM were evaluated based on the C. The pressure–velocity coupling was achieved using the PISO algorithm, while the energy equation was employed to evaluate both the temperature field and the total material fraction (TMF). In the governing equations, conduction and convection effects were accounted for within the momentum and energy formulations, which were discretized using a first-order upwind approach for convective terms and a second-order central difference scheme for diffusive terms. Temporal discretization was performed with the Euler method, applying an adaptive time step to keep the Courant number below 1, thereby ensuring numerical stability and accuracy. The Al□O□ foam region saturated with nano-enhanced PCM is modeled under the local thermal equilibrium (LTE) assumption. Accordingly, a single energy equation is solved for the porous domain using effective (volume-averaged) thermophysical properties, implying that the solid foam matrix and the pore-filling PCM share the same local temperature. This assumption is considered reasonable for the present configuration due to the high thermal conductivity of the Al□O□ skeleton, the small characteristic pore length scale, and the large interfacial area that promote strong local heat exchange. Under LTE, any potential solid–PCM temperature lag within the porous insert is not resolved explicitly and is instead represented through the effective-property formulation.

An essential step in CFD modeling is to ensure mesh independence, which is verified by performing simulations with multiple grid resolutions and comparing the resulting temperature values and heat transfer rates. The mesh that produces stable and consistent results with the coarsest grid is considered adequate, as it balances computational efficiency with solution accuracy. In the present work, a mesh independence study was conducted for a specific C-rate 2 and porosity 0.9. The outcomes of this assessment, presented in Figure□2 and Table 3, demonstrate how mesh refinement influences the maximum temperature of the NPCM at a state

of charge (SOC) of 0%. Table 3 shows the maximum temperatures for various mesh resolutions. The case with 140,000 elements provides stable and precise results for capturing the PCM's thermal behavior.

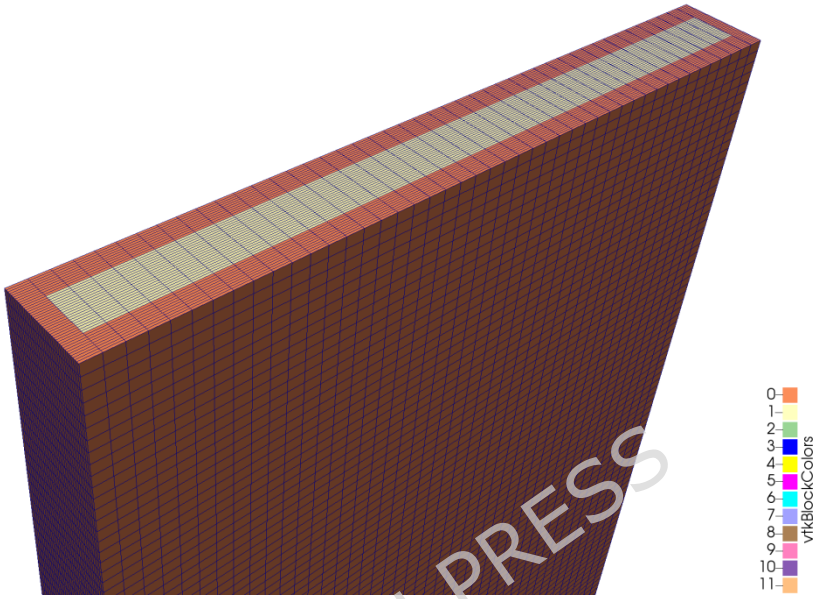

Figure 2: Structured mesh configuration for the pouch-type LIC and housing components.

Table 3: The maximum temperature value for different mech size.

Cell number	T_{max} (C)
60,000	62.716
100,000	61.951
140,000	61.483
220,000	61.273
340,000	61.112

Since this research is purely numerical, it is essential to validate the model against experimental data or previously published numerical results. For validation purposes, the results of the present work were compared with those reported in the experimental study [71], which investigated the thermal behavior of a PCM-porous system used to cool an inclined photovoltaic (PV) panel, through both experimental and numerical approaches. Figure 3a presents a comparison of the

average temperature between the two studies over a 24-hour period. In addition, to strengthen the credibility of our study, the predicted maximum temperature is compared with Ref. [72] over various C-rates. According to the results, the error between our model and the reference studies is within an acceptable range.

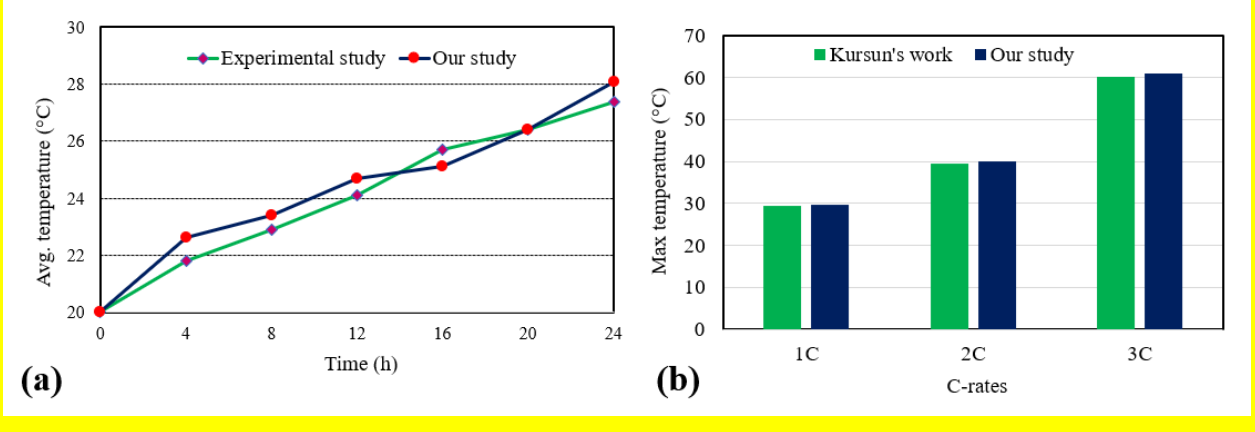

Figure 3: Comparison of the present simulation results: (a) liquid-phase average (LPA), where the green curve represents the present study and the blue curve corresponds to Juan Duan [71]; and (b) maximum temperature used for code validation [72].

5 Results and Discussions

In this study, we investigated the effects of housing geometry and Al_2O_3 foam on the thermal behavior and BTMS of a large-format pouch-type lithium-ion battery during the discharge process at different C-rates (0.5C, 1C, 1.5C, and 2C), as commonly used in EVs. For this purpose, the battery was enclosed within a porous medium composed of Al_2O_3 with a constant pore diameter of 0.2 mm and varying porosities (ε = 0.90, 0.92, 0.94, 0.96, and 0.98) filled with NPCMs. The presence of the Al_2O_3 foam around the battery increases the surface area and thermal conductivity, thereby enhancing convective heat transfer and improving the overall thermal stability and performance of the lithium-ion battery. The NPCM used in this study consisted of n-octadecane as the PCM combined with copper nanoparticles. N-octadecane exhibits effective thermal regulation near its melting temperature (28□°C) by undergoing phase transition and utilizing its latent heat; however, its inherently low thermal conductivity remains a drawback, limiting its heat dissipation capability. To address this limitation, copper nanoparticles with high thermal conductivity were incorporated into the PCM as an effective approach to control and reduce the temperature of the battery during the charge–discharge cycles. To comprehensively analyze the

thermal performance, the variations of average and maximum temperatures, the total melting fraction (TMF%), and the temperature contours within the battery were examined.

As illustrated in Fig. 4, for all C-rates, the average temperature of the lithium-ion battery rises rapidly to approximately 28 °C (the melting temperature of the PCM) as the state of charge (SOC) decreases from 100 % to 95 %. This behavior occurs because the heat generated by the battery is initially absorbed as sensible heat by the PCM (n-octadecane) until its melting point is reached. Beyond this point, from SOC 95 % to 0 % at a C-rate of 0.5, SOC 95 % to 10 % at a C-rate of 1, SOC 95 % to 20 % at a C-rate of 1.5, and SOC 95 % to 40 % at a C-rate of 2, the slope of the temperature curves decreases significantly for all porosities. This reduction in slope is attributed to the phase change of the PCM, during which the latent heat absorbed by the PCM mitigates further temperature rise by transforming the material from a solid to a liquid state. Toward the final stage of the discharge process, the average temperature again increases rapidly for all C-rates except 0.5. This is because, at this stage, most of the PCM has fully melted and can no longer absorb heat through latent heat storage, resulting in a temperature increase. However, for a C-rate of 0.5, the average temperature remains nearly constant at approximately 28.4 °C from SOC 10 % until the end of the discharge process.

On the other hand, an examination of the average temperature for all cases with the same C-rate reveals that an increase in porosity results in a higher average temperature. As discussed previously, this behavior occurs because increasing porosity reduces the effective foam surface area, thereby lowering the overall thermal conductivity of the porous medium. Overall, the average temperature curves exhibit a clear and consistent trend (see Fig. 5). As shown, both higher porosity and higher C-rates lead to an increase in the average temperature. Furthermore, a more detailed analysis indicates that the rise in average temperature between C-rates of 1.5 and 2 is more pronounced than in the other intervals across all porosity values.

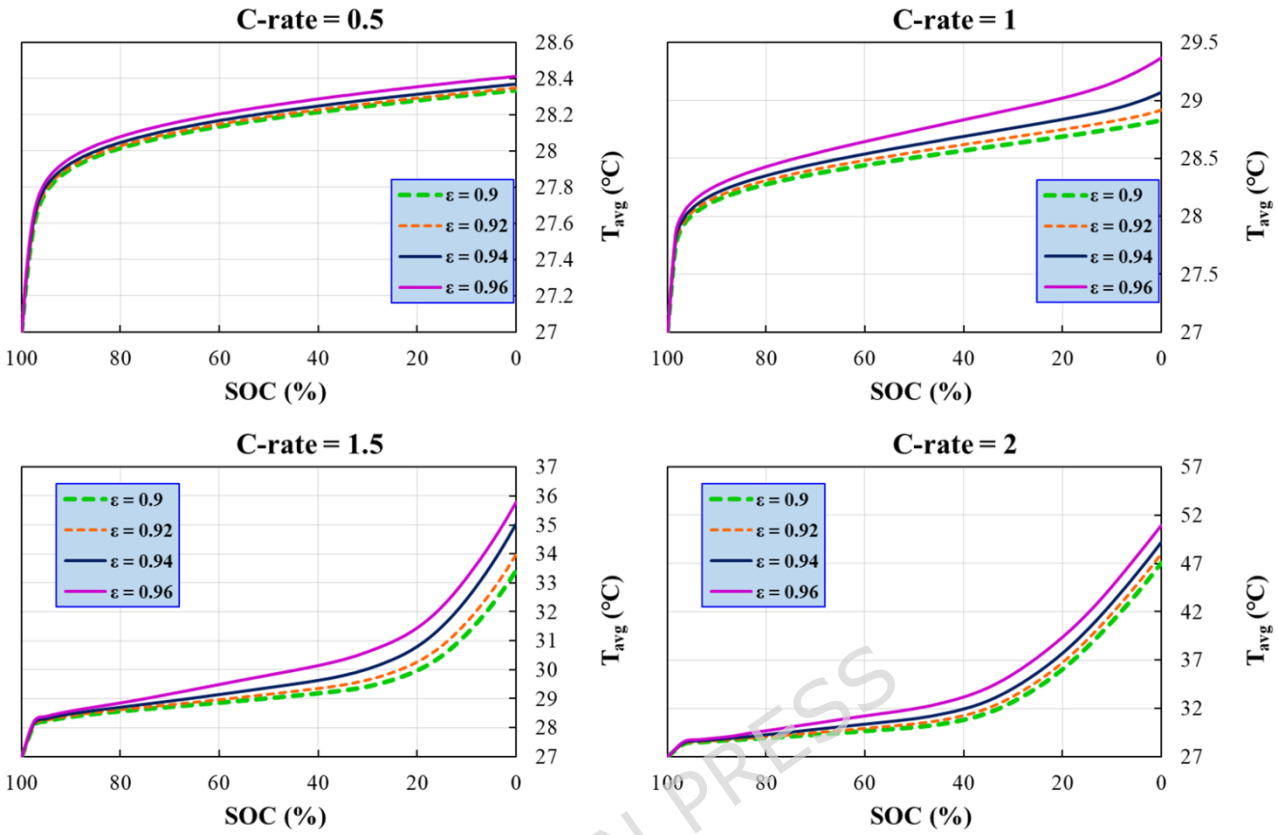

Figure 4: The average temperature versus SOC for various porosities and C-rates.

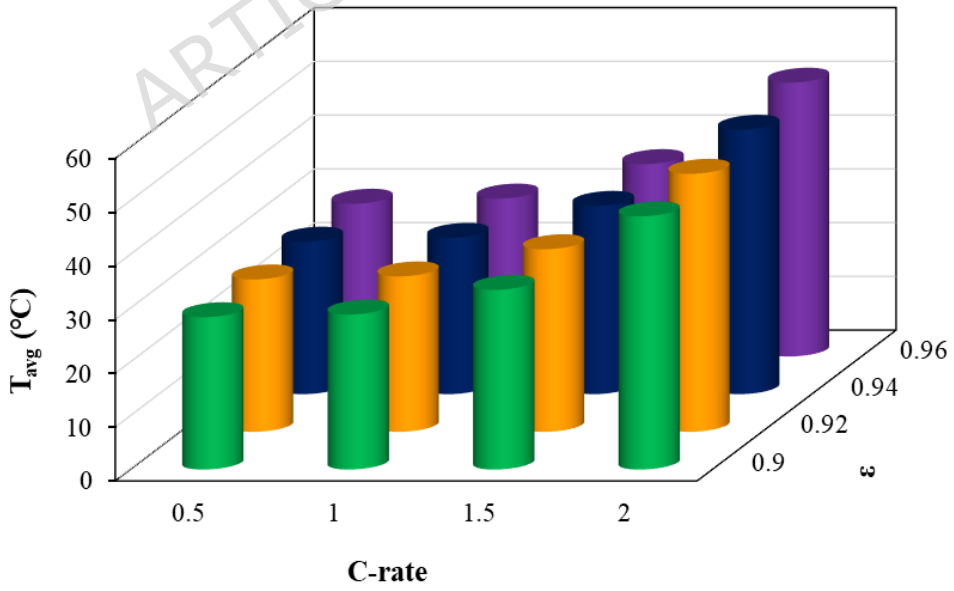

Figure 5:Variation of average temperature at SOC %=0 under different porosity levels and C-rates.

Similar to the trend observed for the average temperature curves, the maximum temperature for all cases rises sharply at the beginning of the discharge process. For the cases with a C-rate of 0.5, after reaching approximately 28□°C, the maximum temperature continues to increase at a relatively small slope, ultimately reaching about 38.5□°C by the end of the discharge (see Fig. 6). However, for the other C-rates (1, 1.5, and 2), the maximum temperature curves exhibit a nearly constant plateau in the mid-region of the discharge process, specifically from SOC 95□% to 20□%, 95□% to 40□%, and 95□% to 50□% for C-rates of 1, 1.5, and 2, respectively. As explained earlier, this plateau corresponds to the phase change of the PCM, during which latent heat absorption mitigates further temperature rise. Furthermore, increasing both the porosity and the C-rate results in higher maximum temperatures. As shown in Fig.□7, the influence of these two parameters on the maximum temperature is evident. The rise in maximum temperature between C-rates of 0.5 and 1 is relatively small; however, as the C-rate increases from 1 to 1.5 and 2, the differences become significantly larger. It should be noted that, for different C-rates, the same SOC corresponds to different absolute discharge times because higher C-rates shorten the total discharge duration. Therefore, comparisons in Figure 6 are performed at identical SOC levels rather than at identical times. This approach ensures that the thermal response is evaluated at the same electrochemical state of the battery, while time-dependent temperature evolution is analyzed separately.

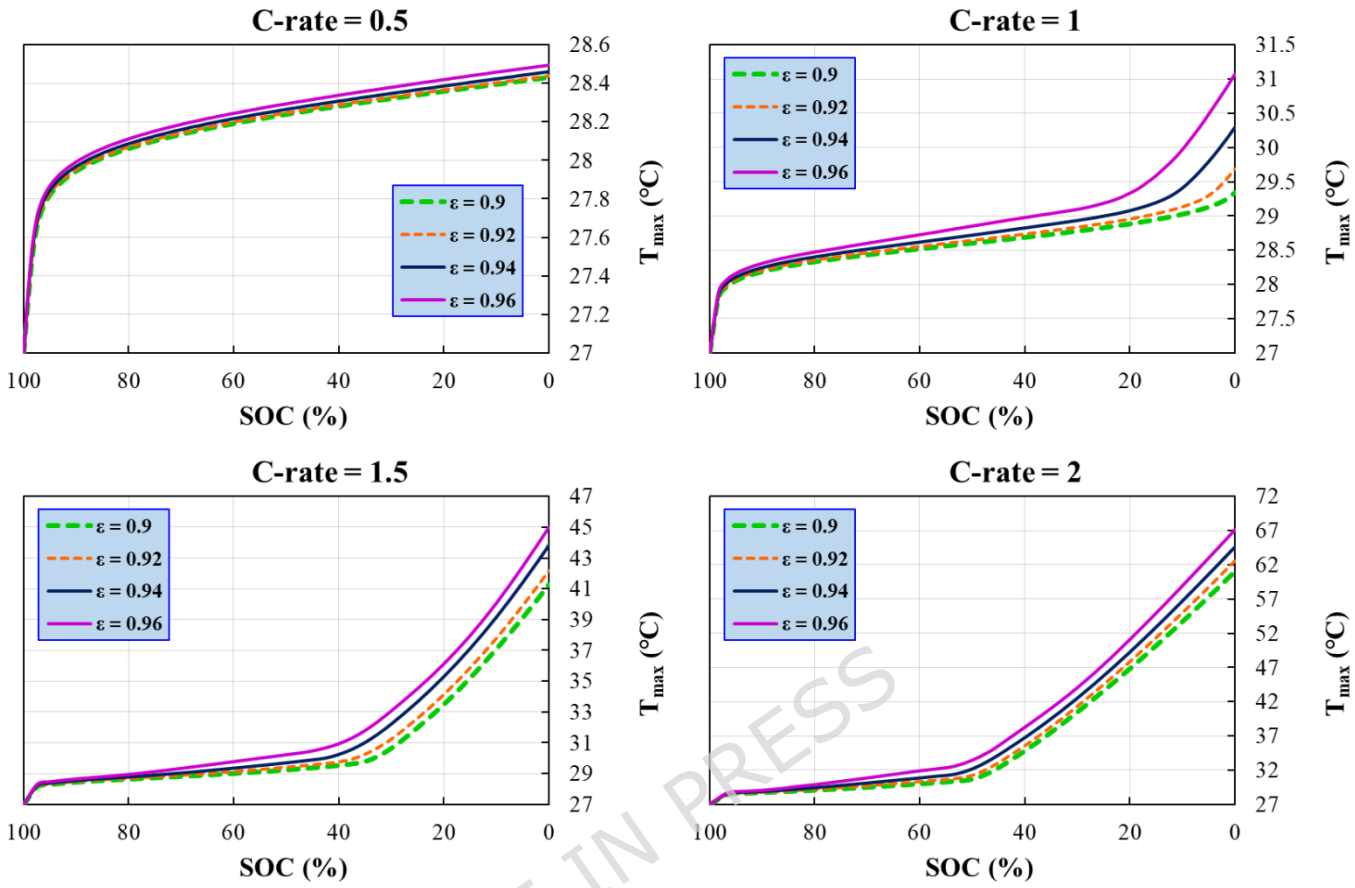

Figure 6:The maximum temperature versus SOC for various porosities and C-rates.

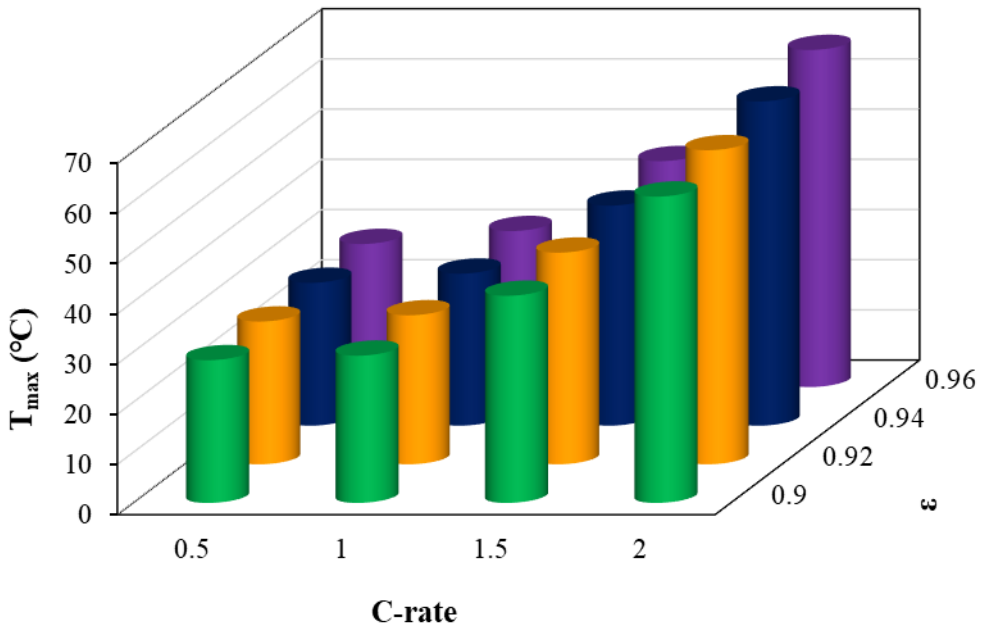

Figure 7: Variation of maximum temperature at SOC %=0 under different porosity levels and C-rates.

In addition to peak and average temperature, the spatial temperature gradient within the pouch cell is an important performance indicator because pronounced non-uniformities can accelerate uneven ageing and introduce local thermal stresses. The temperature contours (Figure 10) show that increasing the C-rate intensifies heat generation and amplifies non-uniformity, with the hottest region remaining concentrated near the cell core while temperatures decrease toward the battery–BTMS interface. This pattern indicates that, under severe discharge, heat removal becomes increasingly constrained by internal heat conduction and the available heat-transfer area. Although the hybrid NPCM–Al□O□ porous medium improves heat spreading through the conductive skeleton and delays temperature rise through latent heat absorption, the contours still show a measurable increase in non-uniformity at the highest C-rates, highlighting the need to evaluate temperature gradients alongside conventional metrics.

Figure 8 further illustrates the combined effects of C-rate and porosity on the temperature field at SOC = 0%. Across all cases, the upper region of the battery remains warmer than other areas. This behavior is consistent with earlier completion of melting in this region, after which the generated heat mainly contributes to sensible heating of the liquid PCM rather than further phase change, reducing the local contribution of latent heat buffering. For a fixed C-rate, decreasing porosity (i.e., increasing the amount of Al□O□ foam) lowers the overall temperature level due to the higher

effective thermal conductivity, which enhances heat transfer within the BTMS. The contours also show that, with greater foam content, the warm region shifts toward the cell center, particularly at lower C-rates, reflecting more effective lateral heat spreading. As the C-rate increases, the temperature field becomes more uniformly elevated throughout the thickness, and the combined effect of higher C-rate and higher porosity results in the highest overall temperatures.

Overall, the contour results confirm that higher porosity promotes a warmer top region associated with earlier PCM liquefaction, whereas increasing Al□O□ foam content enhances effective thermal conductivity, reduces the cell temperature level, and redistributes the warm region toward the interior.

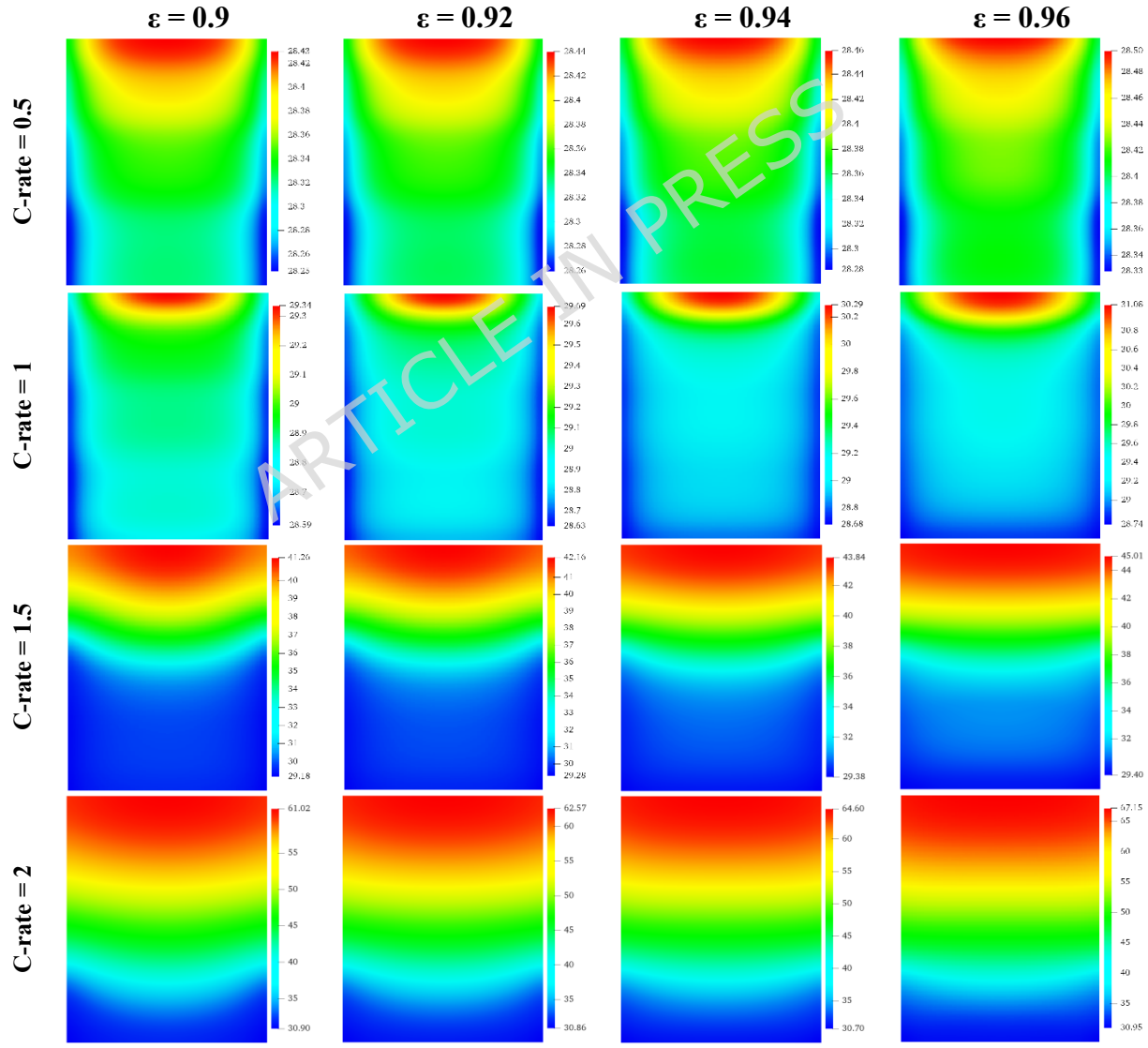

Figure 8:The temperature distribution of LIB at SOC=0% for specimens with various porosities and C-rates.

After analyzing the average and maximum temperatures and temperature contours with respect to SOC, the evaluation of the total melting fraction (TMF□%) provides additional insights into the thermal behavior and BTMS performance of the pouch-type lithium-ion battery. As shown in Fig.□9, the TMF□% remains at zero at the beginning of the discharge process. This initial stage corresponds to the period during which the heat generated by the battery is absorbed as sensible heat by the PCM without inducing a phase change. As the discharge progresses, the TMF□% increases for almost all cases. This behavior is expected because, with the accumulation of heat, a larger proportion of the PCM undergoes a phase transition from solid to liquid. Furthermore, the rate of this phase change becomes more pronounced as the C-rate increases. As observed, for cases with a C-rate of 2, the TMF□% reaches nearly 100□%, indicating that the entire PCM has transitioned from the solid to the liquid state and can no longer absorb additional heat. In contrast, increasing the porosity results in a slightly lower TMF□%. This occurs because higher porosity allows for a larger volume of PCM, so a greater amount of PCM remains partially un-melted. However, as shown in Fig.10, the influence of porosity on TMF□% is relatively small compared to the effect of the C-rate. It can be concluded that the impact of increasing the C-rate on TMF□% is more significant than that of porosity. It is also noteworthy that the change in TMF□% between C-rates 0.5 and 1 is less pronounced than the change between C-rates 1.5 and 2. This is because increasing the C-rate beyond 1.5 leads to a phase transition in more than 80□% of the PCM, whereas at a C-rate of 2 nearly all of the PCM undergoes a complete phase change.

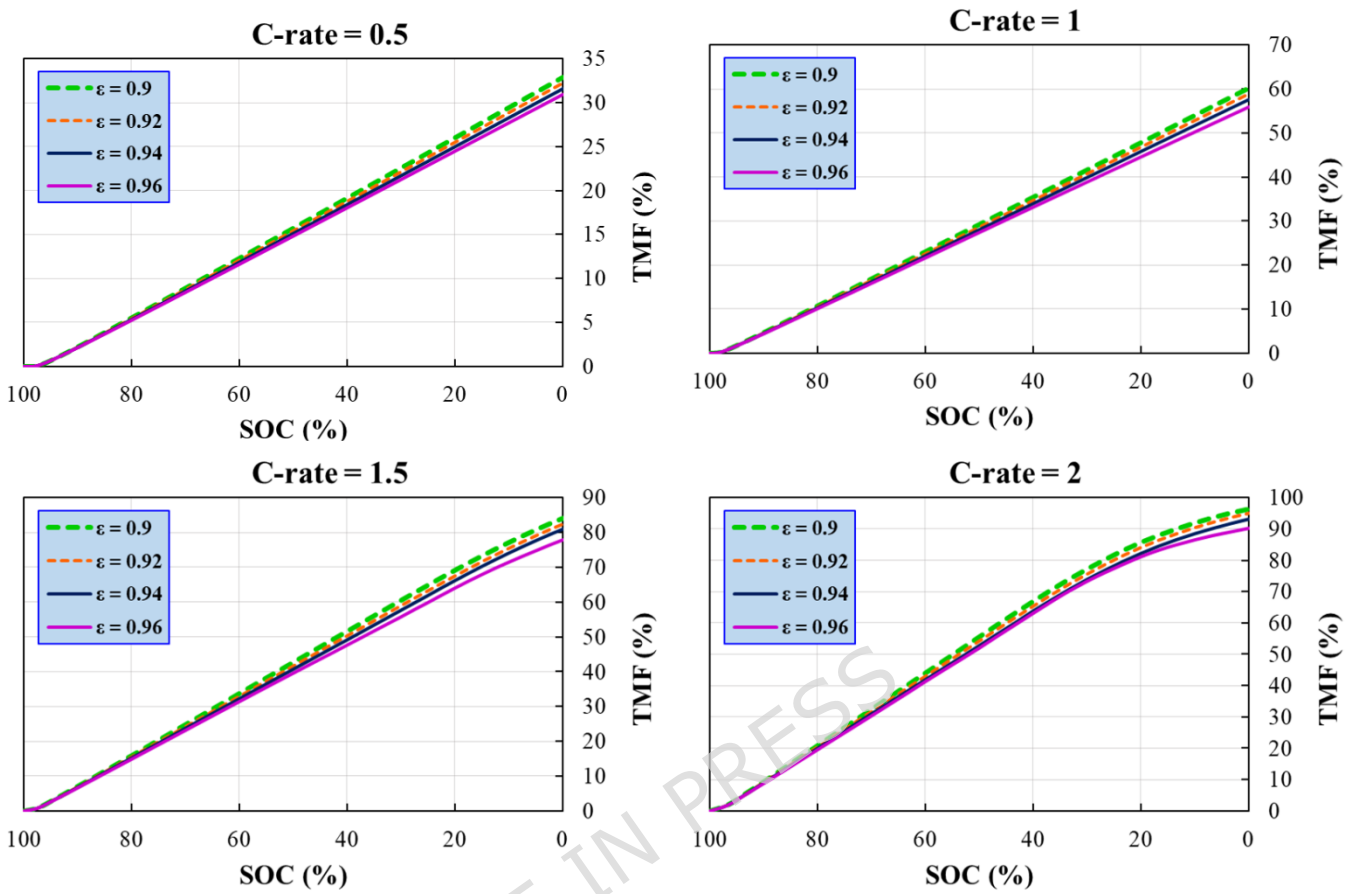

Figure 9: The TMF% values versus SOC for various porosities and C-rates.

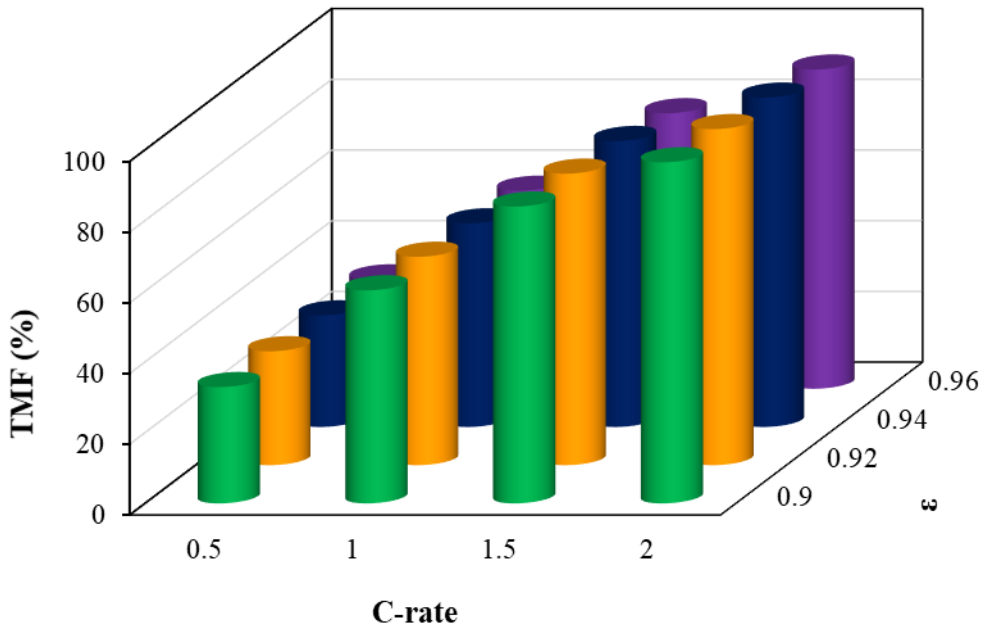

Figure 10:Variation of TMF% at SOC %=0 under different porosity levels and C-rates.

6 Conclusion

In this study, a novel battery thermal management system (BTMS) was developed and numerically analyzed for large-format prismatic lithium-ion batteries commonly used in electric vehicles. The system integrates Al_2O_3 foam with a nano-enhanced phase change material (NPCM) composed of n-octadecane and copper nanoparticles. This hybrid configuration was designed to overcome the low thermal conductivity of conventional PCMs while taking advantage of their latent heat storage capability. Simulations were conducted for various C-rates (0.5C, 1C, 1.5C, and 2C) and porosities (0.90, 0.92, 0.94, 0.96, and 0.98) to evaluate its impact on the battery's thermal performance. The results demonstrate that the proposed system effectively controls the temperature of the battery during the discharge process. At the beginning of discharge, heat is absorbed as sensible heat by the PCM until its melting point (~28□°C) is reached. As the discharge progresses, the phase change of the PCM significantly slows down the temperature rise due to latent heat absorption. With higher C-rates, the heat generation intensifies, causing the melting process to complete earlier, especially at a C-rate of 2 where almost 100□% of the PCM transitions to the liquid state. Porosity also plays a key role: lower porosity (greater foam content) improves effective thermal

conductivity, enhances heat transfer, reduces peak temperatures, and shifts hot spots from the battery surface to the center.

Analysis of the average and maximum temperature profiles, total melting fraction (TMF□%), and temperature contours confirmed that both C-rate and porosity strongly influence thermal behavior. The Al_2O_3 foam redistributes heat more uniformly, while copper nanoparticles significantly improve the PCM's thermal conductivity, resulting in improved stability and reduced risk of overheating. Overall, this study shows that combining Al_2O_3 foam with NPCMs offers an efficient and passive BTMS solution for high-capacity prismatic lithium-ion batteries. This design enhances safety, prolongs battery lifespan, and improves performance, making it a promising approach for electric vehicle applications where thermal management is critical. Future work should focus on experimental validation and optimization of nanoparticle concentration to further enhance heat transfer without compromising latent heat storage.

Data Availability Statement

The datasets used and/or analyzed during the current study are available from the corresponding author upon reasonable request.

Funding Statement

The authors extend their appreciation to the Deanship of Research and Graduate Studies at King Khalid University for funding this work through Large Research Project under grant number RGP2/39/47. This research was funded by Princess Nourah bint Abdulrahman University Researchers Supporting Project number (PNURSP2026R827), Princess Nourah bint Abdulrahman University, Riyadh, Saudi Arabia.

Acknowledgment

The authors extend their appreciation to the Deanship of Research and Graduate Studies at King Khalid University for funding this work through Large Research Project under grant number RGP2/39/47. This research was funded by Princess Nourah bint Abdulrahman University Researchers Supporting Project number (PNURSP2026R827), Princess Nourah bint Abdulrahman University, Riyadh, Saudi Arabia.

Author Contributions Statement

Fares Suliaman Alromithy: Conceptualization, Formal Analysis, Resources, Investigation, Writing – Original Draft, Writing – Review & Editing

Ali B. M. Ali: Conceptualization, Software, Investigation, Validation, Writing – Original Draft, Writing – Review & Editing

Omar J. Alkhatib: Methodology, Software, Investigation, Visualization, Writing – Original Draft, Writing – Review & Editing

Pradeep Kumar Singh: Conceptualization, Methodology, Investigation, Writing – original draft, Writing – Review & Editing

Shimaa A. Hussien: Funding Acquisition, Investigation, Resources, Data Curation, Writing – Original Draft, Writing – Review & Editing

Hamdi Ayed: Funding Acquisition, Methodology, Investigation, Visualization, Writing – Original Draft, Writing – Review & Editing

Farzona Tursunzoda: Conceptualization, Software, Investigation, Writing – Original Draft, Writing – Review & Editing

Mahidzal Dahari: Conceptualization, Validation, Supervision, Project Administration, Writing – Original Draft, Writing – Review & Editing

Ibrahim Mahariq: Resources, Data Curation, Supervision, Project Administration, Writing – Original Draft, Writing – Review & Editing

7 References

1. Petroleum, B., 2020. Statistical review of world energy 2021. *URL: https://www. bp. com/content/dam/bp/business-sites/en/global/corporate/pdfs/energyeconomics/statistical-review/bp-stats-review-2021-full-report. pdf*.
2. Hussien, S.A., Ali, A.B., Rahmani, Y. and Mahariq, I., 2025. Thermal management system of LED headlights based on the active cooling system of water and nano-encapsulated phase change material. *Case Studies in Thermal Engineering*, p.107011.
3. Ahmed, Z., Ali, A.B., AlKhatib, O.J., Mahariq, I., Kriaa, K. and Saif, V., 2025. Synergistic effects of CTAB and low salinity brines on asphaltene behavior and emulsion stability in clay rich sandstone reservoirs. *Scientific Reports*, *15*(1), p.39713.
4. Golab, E., Goudarzi, S., Kazemi-Varnamkhasti, H., Amigh, H., Ghaemi, F., Baleanu, D. and Karimipour, A., 2021. Investigation of the effect of adding nano-encapsulated phase change material to water in natural convection inside a rectangular cavity. *Journal of Energy Storage*, *40*, p.102699.
5. Hwang, F.S., Confrey, T., Reidy, C., Picovici, D., Callaghan, D., Culliton, D. and Nolan, C., 2024. Review of battery thermal management systems in electric vehicles. *Renewable and Sustainable Energy Reviews*, *192*, p.114171.
6. Ahmed, Z., Ali, A.B., AlKhatib, O.J. and Mahariq, I., 2025. Melting behavior in a finned PCM solar thermal receiver/storage unit: a numerical study of heat load and orientation effects. *Energy Reports*, *14*, pp.2927-2938.
7. Liu, Y., Bao, Y., Jiang, S., Ren, Q., Liu, Y. and Li, T., 2026. Sustainable Rubberized Concrete-Filled Square Steel Tubular Columns Under Eccentric Compression. *Materials*, *19*(2), p.250.

8. Siddique, A.R.M., Mahmud, S. and Van Heyst, B., 2018. A comprehensive review on a passive (phase change materials) and an active (thermoelectric cooler) battery thermal management system and their limitations. *Journal of Power Sources*, *401*, pp.224-237.
9. Gungor, S. and Lorente, S., 2024. PCM-based passive cooling solution for Li-ion battery pack, a theoretical and numerical study. *Applied Thermal Engineering*, *257*, p.124262.
10. Motlagh, S.Y., Golab, E. and Sadr, A.N., 2019. Two-phase modeling of the free convection of nanofluid inside the inclined porous semi-annulus enclosure. *International Journal of Mechanical Sciences*, *164*, p.105183.
11. Hussien, S.A., Ali, A.B., Alkhatib, O.J. and Mahariq, I., 2025. Enhanced passive thermal management of lithium-ion batteries with conical cylindrical chamber incorporating various phase change materials. *Scientific Reports*, *15*(1), p.35675.
12. Jiang, G., Huang, J., Liu, M. and Cao, M., 2017. Experiment and simulation of thermal management for a tube-shell Li-ion battery pack with composite phase change material. *Applied Thermal Engineering*, *120*, pp.1-9.
13. Yu, Z., Zhang, J. and Pan, W., 2023. A review of battery thermal management systems about heat pipe and phase change materials. *Journal of Energy Storage*, *62*, p.106827.
14. Shahjalal, M., Shams, T., Islam, M.E., Alam, W., Modak, M., Hossain, S.B., Ramadesigan, V., Ahmed, M.R., Ahmed, H. and Iqbal, A., 2021. A review of thermal management for Li-ion batteries: Prospects, challenges, and issues. *Journal of energy storage*, *39*, p.102518.
15. Fan, R., Zheng, N. and Sun, Z., 2021. Evaluation of fin intensified phase change material systems for thermal management of Li-ion battery modules. *International Journal of Heat and Mass Transfer*, *166*, p.120753.
16. Weng, J., He, Y., Ouyang, D., Yang, X., Zhang, G. and Wang, J., 2019. Thermal performance of PCM and branch-structured fins for cylindrical power battery in a high-temperature environment. *Energy Conversion and Management*, *200*, p.112106.
17. Srivastava, G., Nandan, R. and Das, M.K., 2022. Thermal runaway management of Li ion battery using PCM: a parametric study. *Energy Conversion and Management: X*, *16*, p.100306.
18. Hussien, S.A., Ali, A.B., Alkhatib, O.J., Hamedian, A. and Mahariq, I., 2025. Enhancing battery thermal management system using the emulsion of encapsulated phase change material and water in a mini helical tube. *Scientific Reports*.
19. Vahedi, B., Golab, E., Sadr, A.N. and Vafai, K., 2022. Thermal, thermodynamic and exergoeconomic investigation of a parabolic trough collector utilizing nanofluids. *Applied Thermal Engineering*, *206*, p.118117.
20. Sun, Z., Fan, R., Yan, F., Zhou, T. and Zheng, N., 2019. Thermal management of the lithium-ion battery by the composite PCM-Fin structures. *International Journal of Heat and Mass Transfer*, *145*, p.118739.
21. Faraji, H., Yıldız, Ç., Arshad, A., Arıcı, M., Choukairy, K. and El Alami, M., 2023. Passive thermal management strategy for cooling multiple portable electronic components: Hybrid nanoparticles enhanced phase change materials as an innovative solution. *Journal of Energy Storage*, *70*, p.108087.

22. Rashidi, S., Ijadi, A. and Dadashi, Z., 2022. Potentials of porous materials for temperature control of lithium-ion batteries. *Journal of Energy Storage*, *51*, p.104457.
23. Wang, B., Sun, Z.L., Ren, Q.X., Zhu, Y.H. and Wang, J.H., 2026. Analysis of bond performance between square hollow steel tubes and UHTCC interfaces. *Journal of Constructional Steel Research*, *238*, p.110205.
24. Fan, R., Zheng, N. and Sun, Z., 2021. Evaluation of fin intensified phase change material systems for thermal management of Li-ion battery modules. *International Journal of Heat and Mass Transfer*, *166*, p.120753.
25. Chen, H., Abidi, A., Hussein, A.K., Younis, O., Degani, M. and Heidarshenas, B., 2022. Investigation of the use of extended surfaces in paraffin wax phase change material in thermal management of a cylindrical lithium-ion battery: Applicable in the aerospace industry. *Journal of Energy Storage*, *45*, p.103685.
26. Weng, J., Ouyang, D., Yang, X., Chen, M., Zhang, G. and Wang, J., 2020. Optimization of the internal fin in a phase-change-material module for battery thermal management. *Applied Thermal Engineering*, *167*, p.114698.
27. Sun, Z., Fan, R. and Zheng, N., 2021. Thermal management of a simulated battery with the compound use of phase change material and fins: Experimental and numerical investigations. *International Journal of Thermal Sciences*, *165*, p.106945.
28. Dagdevir, T. and Ding, Y., 2024. Numerical investigation of battery thermal management by using helical fin and composite phase change material. *Journal of Energy Storage*, *75*, p.109674.
29. Mansir, I.B., Sinaga, N., Farouk, N., Aljaghtham, M., Diyoke, C. and Nguyen, D.D., 2022. Numerical simulation of dimensions and arrangement of triangular fins mounted on cylindrical lithium-ion batteries in passive thermal management. *Journal of Energy Storage*, *50*, p.104392.
30. Choudhari, V.G., Dhoble, A.S. and Panchal, S., 2020. Numerical analysis of different fin structures in phase change material module for battery thermal management system and its optimization. *International Journal of Heat and Mass Transfer*, *163*, p.120434.
31. Zhang, F., Lu, F., Liang, B., Zhu, Y., Gou, H., Xiao, K. and He, Y., 2023. Thermal performance analysis of a new type of branch-fin enhanced battery thermal management PCM module. *Renewable Energy*, *206*, pp.1049-1063.
32. Liu, H., Jin, C., Li, H. and Ji, Y., 2023. A numerical study of PCM battery thermal management performance enhancement with fin structures. *Energy Reports*, *9*, pp.1793-1802.
33. Xiang, X., Routsi, A.M., Nagarajan, R., Wang, Q., Yang, R., Esfahani, I.C., Hoffman, D. and Sun, H., 2026. Numerical and experimental investigation of a hybrid battery thermal management system for high-rate applications. *Journal of Energy Storage*, *141*, p.119081.
34. Motlagh, S.Y., Golab, E. and Sadr, A.N., 2019. Two-phase modeling of the free convection of nanofluid inside the inclined porous semi-annulus enclosure. *International Journal of Mechanical Sciences*, *164*, p.105183.
35. Zehao, Z.H.A.O., Jinlong, Z.H.A.N.G. and Yuhong, D.O.N.G., 2023. Heat transfer models for porous media in porous-walled turbulent flows. *Acta Aerodynamica Sinica*, *42*(1), pp.45-54.

36. Izadi, M., Javanahram, M., Zadeh, S.M.H. and Jing, D., 2020. Hydrodynamic and heat transfer properties of magnetic fluid in porous medium considering nanoparticle shapes and magnetic field-dependent viscosity. *Chinese Journal of Chemical Engineering*, *28*(2), pp.329-339.
37. Faraz, M.R., Ahmadi, H., Liaghat, G., Vahid, S., Razmkhah, O. and Tarafdar, A., 2022. Energy absorption assessment of bio-mimicked hybrid Al/PP sandwich tube: experimental and Numerical Investigation. *Thin-Walled Structures*, *181*, p.110116.
38. Ranjbaran, Y.S., Haghparast, S.J., Shojaeefard, M.H. and Molaeimanesh, G.R., 2020. Numerical evaluation of a thermal management system consisting PCM and porous metal foam for Li-ion batteries: YS Ranjbaran et al. *Journal of Thermal Analysis and calorimetry*, *141*(5), pp.1717-1739.
39. Sudhakaran, S., Terese, M., Mohan, Y., Thampi, A.D. and Rani, S., 2023. Influence of various parameters on the cooling performance of battery thermal management systems based on phase change materials. *Applied Thermal Engineering*, *222*, p.119936.
40. Heyhat, M.M., Mousavi, S. and Siavashi, M., 2020. Battery thermal management with thermal energy storage composites of PCM, metal foam, fin and nanoparticle. *Journal of Energy Storage*, *28*, p.101235.
41. Mehrabi-Kermani, M., Houshfar, E. and Ashjaee, M., 2019. A novel hybrid thermal management for Li-ion batteries using phase change materials embedded in copper foams combined with forced-air convection. *International Journal of Thermal Sciences*, *141*, pp.47-61.
42. Zhang, Z., Cheng, J. and He, X., 2017. Numerical simulation of flow and heat transfer in composite PCM on the basis of two different models of open-cell metal foam skeletons. *International Journal of Heat and Mass Transfer*, *112*, pp.959-971.
43. Tarafdar, A., Liaghat, G., Ahmadi, H., Razmkhah, O., Charandabi, S.C., Faraz, M.R. and Pedram, E., 2021. Quasi-static and low-velocity impact behavior of the bio-inspired hybrid Al/GFRP sandwich tube with hierarchical core: experimental and numerical investigation. *Composite Structures*, *276*, p.114567.
44. Daneshazarian, R., Antoun, S. and Dworkin, S.B., 2021. Performance assessment of nano-enhanced phase change material for thermal storage. *International Journal of Heat and Mass Transfer*, *173*, p.121256.
45. Vali, P.M. and Murali, G., 2024. Experimental study on thermal management of nano-enhanced phase change material integrated battery pack. *ASME Journal of Heat and Mass Transfer*, *146*(3), p.032401.
46. Laghari, I.A., Bhutto, Y.A., Koondhar, M.A. and Shah, S.A.A., 2023. Application of nano-enhanced PCMs in electronic devices. In *Nano Enhanced Phase Change Materials: Preparation, Properties and Applications* (pp. 167-199). Singapore: Springer Nature Singapore.
47. He, X., Wang, Y., Cui, K., Tian, Y., Yu, C. and Wang, X., 2025. Controllable wetting characteristics of hierarchically structured surfaces. *Journal of Colloid and Interface Science*, p.138961.
48. Pan, M. and Zhong, Y., 2018. Experimental and numerical investigation of a thermal management system for a Li-ion battery pack using cutting copper fiber sintered skeleton/paraffin composite phase change materials. *International Journal of Heat and Mass Transfer*, *126*, pp.531-543.
49. Karimi, G., Azizi, M. and Babapoor, A., 2016. Experimental study of a cylindrical lithium ion battery thermal management using phase change material composites. *Journal of Energy Storage*, *8*, pp.168-174.

50. Zou, D., Ma, X., Liu, X., Zheng, P. and Hu, Y., 2018. Thermal performance enhancement of composite phase change materials (PCM) using graphene and carbon nanotubes as additives for the potential application in lithium-ion power battery. *International Journal of Heat and Mass Transfer*, *120*, pp.33-41.
51. Righetti, G., Savio, G., Meneghello, R., Doretti, L. and Mancin, S., 2020. Experimental study of phase change material (PCM) embedded in 3D periodic structures realized via additive manufacturing. *International Journal of Thermal Sciences*, *153*, p.106376.
52. Li, Z., Tavakoli, F., El-Shafay, A.S., Liu, X., Mousa, M. and Heidarshenas, B., 2022. Economic cost and technical efficiency analysis of thermal management of a triple pack of lithium-ion battery with forced airflow and nano-phase change materials. *Journal of Power Sources*, *542*, p.231715.
53. Habibishandiz, M. and Saghir, M.Z., 2022. A critical review of heat transfer enhancement methods in the presence of porous media, nanofluids, and microorganisms. *Thermal Science and Engineering Progress*, *30*, p.101267.
54. Esfe, M.H., Bahiraei, M., Hajbarati, H. and Valadkhani, M., 2020. A comprehensive review on convective heat transfer of nanofluids in porous media: Energy-related and thermohydraulic characteristics. *Applied Thermal Engineering*, *178*, p.115487.
55. Zhang, Y., Zhang, K., Wang, J., Qi, Y., Yang, Z. and Mao, Z., Regulating Temperature of a Lifepo4 Lithium-Ion Pouch Cell Using Nano-Enhanced Phase Change Material: A Cfd Simulation. *Available at SSRN 4695705*.
56. Luo, J., Zou, D., Wang, Y., Wang, S. and Huang, L., 2022. Battery thermal management systems (BTMs) based on phase change material (PCM): A comprehensive review. *Chemical Engineering Journal*, *430*, p.132741.
57. Wang, H., Tao, T., Xu, J., Shi, H., Mei, X. and Gou, P., 2022. Thermal performance of a liquid-immersed battery thermal management system for lithium-ion pouch batteries. *Journal of energy storage*, *46*, p.103835.
58. Zhang, Q. and White, R.E., 2007. Calendar life study of Li-ion pouch cells. *Journal of Power Sources*, *173*(2), pp.990-997.
59. Vyas, D., Bhatt, J., Rajput, A., Hotta, T.K., Rammohan, A. and Raghuraman, D.R.S., 2024. Investigation on thermal management of 18650 lithium-ion batteries using nano-enhanced paraffin wax: a combined numerical and experimental study. *Arabian Journal for Science and Engineering*, *49*(11), pp.15565-15582.
60. Zhang, G., Chen, G., Li, P., Xie, Z., Li, Y. and Luo, T., 2024. Cooling performance of a nano phase change material emulsions-based liquid cooling battery thermal management system for high-capacity square lithium-ion batteries. *Fire*, *7*(10), p.371.
61. Kumaresan, N., 2021. Thermal Management of Li-ion batteries by Thermal Barrier Coatings.
62. Paciolla, P. and Papurello, D., 2024. Improved thermal management of Li-ion batteries with phase-change materials and metal fins. *Batteries*, *10*(6), p.190.
63. Kharabati, S. and Saedodin, S., 2024. A systematic review of thermal management techniques for electric vehicle batteries. *Journal of Energy Storage*, *75*, p.109586.

64. Nazar, M.W., Iqbal, N., Ali, M., Nazir, H. and Amjad, M.Z.B., 2023. Thermal management of Li-ion battery by using active and passive cooling method. *Journal of Energy Storage*, *61*, p.106800.

65. Ahmed, Z., Ali, A.B., Khan, Z., Singh, P.K., AlKhatib, O.J., Kriaa, K., Mahariq, I. and Dahari, M., 2026. Control of sludge formation during acidizing through the investigation of acid and oil interactions and emulsion behavior in heavy oils using low salinity water. *Scientific Reports*.

66. Izadi, M., Sheremet, M.A. and Mehryan, S.A.M., 2020. Natural convection of a hybrid nanofluid affected by an inclined periodic magnetic field within a porous medium. *Chinese Journal of Physics*, *65*, pp.447-458.

67. Kilic, G.A., 2023. An experimental analysis on the effects of passive liquid cooling system on thermal management system. *International Journal of Thermofluids*, *18*, p.100370.

68. Al-Yasiri, Q. and Szabó, M., 2023. Numerical analysis of thin building envelope-integrated phase change material towards energy-efficient buildings in severe hot location. *Sustainable Cities and Society*, *89*, p.104365.

69. Gupta, M.K., Rathore, P.K.S., Kumar, R. and Gupta, N.K., 2023. Experimental analysis of clay bricks incorporated with phase change material for enhanced thermal energy storage in buildings. *Journal of Energy Storage*, *64*, p.107248.

70. Meng, X., 2024. Thermal performance assessment of the dynamic rotating latent-energy-storage envelope (DRLESE) during winter. *Case Studies in Thermal Engineering*, *60*, p.104671.

71. Duan, J., 2021. The PCM-porous system used to cool the inclined PV panel. *Renewable Energy*, *180*, pp.1315-1332.

72. Kurşun, B., Toklu, E., Polat, F. and Balta, M., 2024. The effect of outer container geometry on the thermal management of lithium-ion batteries with a combination of phase change material and metal foam. *Journal of Energy Storage*, *80*, p.110227.

Abbreviation Table

Shortened phrase	***The full phrase***
LIB	*Lithium-Ion Battery*
PCM	*Phase Change Material*
NPCM	*Nano-Enhanced Phase Change Material (NPCM)*
BTMS	*Battery Thermal Management System*
TMF	*Total Melting Fraction*
PISO	*Pressure-Implicit with Splitting of Operators*
CFD	*Computational Fluid Dynamics*

FVM	*Finite Volume Method*
PDE	*Partial Differential Equation*

Symbol Table

Nomenclature		***Greek symbols***	
C_p	*Specific heat capacity (J/kg.K)*	ρ	*Density (kg/m^3)*
g	*Gravitational acceleration (m/s^2)*	μ	*Dynamic viscosity (Pa.s)*
k	*Thermal conductivity (W/m.K)*	β	*Thermal expansion coefficient (1/K)*
W	*Battery Width (mm)*	λ	*Error function*
H	*Battery Height (mm)*	φ	*Volume fraction (-)*
Cu	*Copper*	σ	*Stefan-Boltzmann constant (W/m^2. K^4)*
V	*Velocity (m/s)*	ε	*porosity (-)*
K	*Permeability (m^2)*	***Subscript***	
p	*Pressure (Pa)*	*max*	*Maximum*
h	*Convective heat transfer coefficient (W/m^2 .K)*	*min*	*Minimum*
T	*Temperature (□)*	*eff*	*Effective*
u, v, w	*Velocity vector (m/s)*	*avg*	*Average*
x, y, z	*Cartesian coordinates (m)*	*c*	*Cell*

t	*Time (s)*